Structural and Magnetic Characterization of Ni-Co Mixed Ferrite Nanopowders Synthesized via Coprecipitation and Sol-Gel Methods

Gerson Márquez[a,b]* ![ORCID], *Edgar Pérez[b], Vicente Sagredo[b]*

[a]Universidad Tecnológica del Perú, Instituto de Energías Renovables, 04001 Arequipa, Perú.
[b]Universidad de Los Andes, Departamento de Física, 5101 Mérida, Venezuela.

$Ni_{0.5}Co_{0.5}Fe_2O_4$ nanoparticulate powders were synthesized using coprecipitation and sol-gel methods. The crystalline structure of the nanocompounds was determined through X-ray diffraction analysis. The chemical composition of the synthesized nanopowders was analyzed using infrared spectroscopy measurements. The size, morphology, and aggregation of the nanoparticles were determined from electron microscopy images. The magnetic properties of the nanocompounds were studied through magnetization measurements as a function of temperature and applied magnetic field. The synthesized powders consist of aggregates of nanoparticles with mean particle sizes of 24 nm and 43 nm, with those synthesized using the coprecipitation method being smaller. The compounds exhibited a single crystalline phase corresponding to the cubic spinel structure, with a unit cell parameter of approximately 8.35 Å and an inversion parameter with values of 0.94 and 0.95. The synthesized Ni-Co mixed ferrites presented an ordered magnetic behavior below 320 K, with the nanoparticles being in the blocked magnetic regime.

Keywords: *Nanopowders, Coprecipitation, Sol-gel, Ni-Co Ferrite, Magnetic Characterization.*

1. Introduction

Ferrites are magnetic materials that can be used in a wide variety of applications in various fields, such as medicine and electronics[1,2]. In medicine, they can be utilized as magnetic resonance contrast agents to obtain high-resolution medical images. Additionally, they can serve as heating agents to destroy cancerous tumors in magnetic hyperthermia therapy[3,4]. In electronics, they find application in the manufacturing of magnetic field sensors and data storage devices, such as hard drives and magnetic tapes. Moreover, they are utilized in the production of permanent magnets and electronic devices, including inductors, transformers, and signal filters[5].

Reducing the size of materials to the nanoscale can endow them with novel and interesting physical and chemical properties that differ significantly from those they present as bulk materials. Unusual phenomena such as quantum confinement, or behaviors such as superparamagnetism, arise from the material's nanoscale dimensions. The high surface-to-volume ratio inherent to nanoparticles makes them highly attractive for a variety of applications in biomedicine, catalysis, electronics, sensors, and other fields[3,6]. Ferrite nanoparticles are promising for applications in environmental catalysis due to their high specific surface area, chemical stability, and interesting and unique magnetic properties. Among the potential applications of nanoferrites in environmental catalysis is the removal of organic and inorganic contaminants in water and air. For example, they can be used in treating water contaminated with heavy metals or controlling polluting gas emissions like carbon monoxide and nitrogen oxides that are produced in industries or vehicle

exhaust[7-9]. Additionally, research has been conducted where ferrite nanoparticles have been used to eliminate emerging contaminants such as drugs and personal hygiene products[10].

Among the ferrites with the formula AFe_2O_4, nickel and cobalt ferrites are particularly interesting because they exhibit properties such as high magnetic permeability, high electrical resistivity, and low dielectric loss. Both ferrites crystallize in the spinel structure, which corresponds to a cubic arrangement where ions occupy sites with tetrahedral and octahedral coordination. Specifically, the crystal structure of nickel ferrite ($NiFe_2O_4$) is an inverse spinel, with all the Ni^{2+} cations located in octahedral sites, while the Fe^{3+} ions are positioned between the tetrahedral and octahedral sites[11]. In the case of cobalt ferrite ($CoFe_2O_4$), the structure is a partially inverse spinel, with 60 to 90% of Co^{2+} cations occupying the octahedral sites[12].

As bulk materials, nickel and cobalt ferrites exhibit ferrimagnetic properties at room temperature, where the magnetic ordering is determined by superexchange interactions between metal cations, utilizing O^{2-} anions as intermediates[13]. When considering magnetic properties, nickel and cobalt ferrites exhibit notable differences. $CoFe_2O_4$ stands out as having the highest values of coercivity, remanent magnetization, and saturation magnetization[14]. Additionally, cobalt ferrite is distinguished by its high magnetocrystalline anisotropy[15].

At the nanoscale, nickel and cobalt ferrites can exhibit superparamagnetic behavior when the nanoparticle size is smaller than the superparamagnetic size (D_{SP}), which is 28 nm for $NiFe_2O_4$ and 14 nm for $CoFe_2O_4$[16,17]. Superparamagnetic materials are characterized by the absence of coercivity; however, they can exhibit large saturation magnetizations,

*e-mail: gmarquez@utp.edu.pe

which may be comparable to those of the bulk material. Superparamagnetism is a characteristic behavior of non-interacting particle systems. Consequently, the aggregation and size dispersion of nanoparticles can impact the superparamagnetic response of the material, resulting in the observation of non-zero coercive fields[18].

The combination of nickel and cobalt ferrites in equal proportions allows for the formation of $Ni_{0.5}Co_{0.5}Fe_2O_4$, which is expected to crystallize in the spinel structure with a high degree of inversion, closely resembling an inverse spinel. Changes in the crystalline structure, as well as the disparity in size and magnetic moment of the Ni^{2+} and Co^{2+} cations, influence the physical properties of the ferrite, such as saturation magnetization and coercivity. There are several methods to synthesize ferrite nanoparticulate powders, including chemical methods such as coprecipitation[19,20], sol-gel[21,22], and autocombustion[23]. These methods are relatively simple and low-cost, utilizing metal precursors such as nitrates and chlorides. While all three methods mentioned are effective for nanoparticle production, coprecipitation and sol-gel methods provide greater control over the composition and size of the nanoparticles.

Several investigations have studied the effect of the substitution of Co by Ni on the properties $CoFe_2O_4$ nanoparticles[14,24,25], as well as the influence of replacing transition metal ions (Zn^{2+}, Mn^{2+}, Co^{3+}, Cr^{3+}) or rare earths ions (Tb^{3+}, Tm^{3+}, Ho^{3+}, Nd^{3+}) in mixed Ni-Co ferrites[26-30]. Various synthesis methods, including coprecipitation[24,31], sol-gel[27-29], ultrasonic technique[26], and sol-gel auto-combustion[30,32,33], have been employed to produce these Ni-Co mixed ferrite nanoparticles. However, there is a lack of research comparing the structural characteristics and magnetic properties of $Ni_{0.5}Co_{0.5}Fe_2O_4$ nanoparticles synthesized using coprecipitation and sol-gel methods. The cationic distribution of this mixed ferrite has been little studied, and no investigations have determined the distribution of Ni^{2+}, Co^{2+}, and Fe^{3+} cations from the material's saturation magnetization at low temperatures, where collinear magnetic ordering can be assumed. Consequently, we consider it interesting to synthesize Ni-Co mixed ferrite nanoparticles using coprecipitation and sol-gel methods to study and compare the structural and magnetic properties of the compounds produced by both synthesis methods. Moreover, given the established correlation between magnetization and the structural inversion degree, we deem it essential to determine the cationic distribution in both synthesized nanoferrites from the saturation magnetization values, which represents a novelty with respect to the reviewed literature.

In this work, $Ni_{0.5}Co_{0.5}Fe_2O_4$ nanoparticulate powders were synthesized using coprecipitation and sol-gel methods. The crystalline structure, chemical composition, morphology, size, aggregation, cationic distribution, and magnetic properties of the synthesized nanoparticles were determined.

2. Experimental

2.1. Synthesis of nanoparticles

$Ni_{0.5}Co_{0.5}Fe_2O_4$ nanoparticles were synthesized using the coprecipitation and sol-gel methods, employing nickel(II) nitrate hexahydrate ($Ni(NO_3)_2 \cdot 6H_2O$), cobalt(II) nitrate hexahydrate ($Co(NO_3)_2 \cdot 6H_2O$), and iron(III) nitrate nonahydrate

($Fe(NO_3)_3 \cdot 9H_2O$) as metal precursors. These metal nitrates were dissolved in deionized water and mixed in appropriate proportions, according to the following chemical equation:

$$Ni(NO_3)_2 \cdot 6H_2O + Co(NO_3)_2 \cdot 6H_2O + 4Fe(NO_3)_3 \cdot 9H_2O + H_2O \rightarrow Ni_{0.5}Co_{0.5}Fe_2O_4 + 49H_2O \quad (1)$$
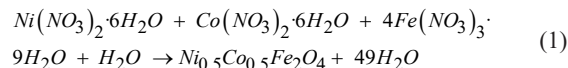
In the coprecipitation method, ammonium hydroxide - NH_4OH (29.66 wt%) was used as the precipitating agent, whereas in the sol-gel synthesis, citric acid ($C_6H_8O_7$) and ethylene glycol ($C_2H_6O_2$) were utilized to promote gel formation. The details of the procedure followed for the synthesis by the coprecipitation and sol-gel methods can be found in two previously published research papers[34,35].

In the synthesis of $Ni_{0.5}Co_{0.5}Fe_2O_4$ nanoparticles, byproducts such as ammonium nitrate ($NH_4(NO_3)$) are generated, as observed in the chemical reaction involved in the synthesis by the coprecipitation method, which is represented in the following chemical equation:

$$Ni(NO_3)_2 \cdot 6H_2O + Co(NO_3)_2 \cdot 6H_2O + 4Fe(NO_3)_3 \cdot 9H_2O + H_2O + 16NH_4OH \rightarrow Ni_{0.5}Co_{0.5}Fe_2O_4 + 57H_2O + 16NH_4(NO_3) \quad (2)$$
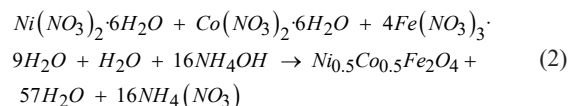
The byproducts generated in the synthesis processes can be eliminated by washing the synthesized powders or by thermal treatments or calcinations[34]. In several investigations that have studied the effect of heat treatment temperature on the crystal structure, size, and physical properties of nanoparticles, it has been reported that the crystallinity of nanometric particles synthesized using methods such as coprecipitation or sol-gel improves as the heat treatment temperature increases[36,37]. Generally, as-synthesized nanoparticles have been found to exhibit low crystallinity[38,39]. To obtain pure Ni-Co mixed ferrite nanocrystals, the powders synthesized using both methods were calcined at 600 °C for 2 hours in an air atmosphere. The thermal treatment involved heating the samples to the calcination temperature at a rate of 1°C/min, followed by spontaneous cooling to room temperature.

2.2. Characterization techniques

The crystalline structure of the synthesized compounds was characterized by analyzing X-Ray Diffraction (XRD) data measured using an INEL CPS 120 powder diffractometer. CuKα radiation was employed in the 2θ range of 15 to 70° with steps of 0.03° and a measurement time of 0.5 s/step. The XRD data was analyzed and processed using the FullProf Suite software. The identification of crystalline phases was performed by comparing the observed diffraction peaks with the Powder Diffraction File (PDF) database. The crystal lattice parameters were determined using the Le Bail refinement method. The average particle sizes were estimated by calculating the crystallite sizes using the Scherrer equation[40]:

$$D_{XRD} = 0.89 \cdot \lambda / (\beta \cdot cos\theta) \quad (3)$$

Where λ represents the X-ray wavelength, β represents the full width at half-maximum (FWHM), and θ represents the Bragg angle of the selected diffraction peak[41].

Structural and Magnetic Characterization of Ni-Co Mixed Ferrite Nanopowders Synthesized via
Coprecipitation and Sol-Gel Methods

3

The chemical composition of the synthesized compounds was analyzed using Fourier-Transform Infrared Spectroscopy (FTIR) measurements conducted on a PerkinElmer spectrophotometer. The measurements were performed in the range of 4500 to 380 cm⁻¹ with samples prepared by dispersing Ni-Co mixed ferrite powders at a concentration of 1.5% in potassium bromide (KBr).

The size, morphology, and aggregation of the nanoparticles were determined from Transmission Electron Microscopy (TEM) and Scanning Electron Microscopy (SEM) images for the Ni-Co mixed ferrites synthesized by the coprecipitation and sol-gel methods, respectively. TEM micrographs were captured using a JEOL JEM 1220 microscope operating at an accelerating voltage of 100 kV, enabling the acquisition of micrographs at a magnification of x40k. The sample was prepared by dispersing a small amount of powdered material in ethanol. Subsequently, a drop of the nanoparticle suspension was placed on a carbon-coated copper grid, allowing the ethanol to evaporate until the nanoparticles were immobilized on the grid. SEM images were captured using a JEOL 6400 microscope equipped with an Oxford Link Isis detector. The micrographs were processed using the DigitalMicrograph software, and more than 300 nanoparticles were measured to evaluate the particle size distribution.

The magnetic properties of the nanoparticles were studied through magnetization measurements performed on a Quantum Design MPMS XL-7 SQUID magnetometer. The magnetization (M) was measured as a function of temperature (T) in the range of 2 to 320 K, applying magnetic fields (H) of 10 and 50 Oe in the zero-field-cooled (ZFC) and field-cooled (FC) modes. The magnetization measurements as a function of the applied magnetic field were conducted at different temperatures by applying magnetic fields up to 5.5 T. Parameters such as coercive field (H_C), saturation magnetization (M_S), and remanent magnetization (M_R) were determined from the M vs. H curves.

3. Results and Discussion

In Figure 1, the X-ray diffractograms of the Ni-Co mixed ferrite samples synthesized using the coprecipitation and sol-gel methods are shown. Both diffraction patterns show peaks that can be identified as corresponding to the NiFe₂O₄ (JCPDS: 86-2267) and CoFe₂O₄ (JCPDS: 22-1086) standards. This indicates that the two compounds crystallized in the cubic spinel structure, which is characteristic of ferrites with the formula AFe₂O₄. Furthermore, no additional peaks suggesting the formation of secondary crystalline phases are observed. The indexing of the observed diffraction peaks is presented in Figure 1, identifying the highest intensity peaks located around 35.4° as corresponding to the (3 1 1) crystallographic planes. When comparing the two diffractograms, it is observed that the diffraction peaks of pattern (a) are broader than those of pattern (b), suggesting that the particles of the sample synthesized by the coprecipitation method are smaller than those produced by the sol-gel method. This is confirmed by the results of the crystalline domain sizes obtained by applying the Scherrer equation and considering the Bragg angle and the FWHM of the (3 1 1) peaks. It was found that the crystallites have sizes of 16.5 nm and 29.5 nm for the Ni₀.₅Co₀.₅Fe₂O₄ ferrite synthesized by the coprecipitation
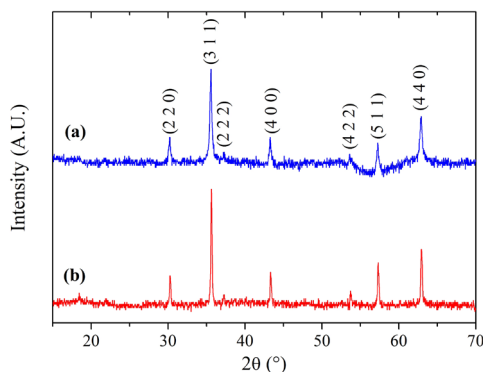
Figure 1. X-ray diffractograms of Ni₀.₅Co₀.₅Fe₂O₄ nanopowders synthesized by the (a) coprecipitation and (b) sol-gel methods.

and sol-gel methods, respectively. The difference in size of the crystallites reveals effects generated by the chemical processes involved in the two synthesis methods on the nanoparticle size. In the coprecipitation method, the formation of nanoparticles occurs rapidly due to the chemical reaction between the metal precursors and the precipitating agent in the solution. The rapid formation of particle nuclei can limit growth and lead to the formation of smaller particles[42,43]. On the other hand, in the sol-gel method, the particles form through hydrolysis and condensation reactions of the precursors, allowing for a longer growth time and, therefore, the possibility of obtaining larger particles[44].

Through the Le Bail refinement, unit cell parameters (a) of 8.353 and 8.359 Å were found for the Ni₀.₅Co₀.₅Fe₂O₄ synthesized by the coprecipitation and sol-gel methods, respectively. These values of a obtained are very close, indicating that the compounds produced by the two synthesis routes have similar structural characteristics. The obtained lattice parameters fall between the known values for NiFe₂O₄, 8.337 Å (JCPDS: 86-2267), and CoFe₂O₄, 8.392 (JCPDS: 22-1086), confirming that it is indeed a Ni-Co mixed ferrite.

Figure 2 shows the FTIR spectra of the two samples of Ni₀.₅Co₀.₅Fe₂O₄ in KBr, where several absorption bands are observed and assigned as follows: the bands at 3424-3440 cm⁻¹ correspond to vibrations of O-H bonds[34], 2831-2837 cm⁻¹ is due to C-H vibrations[45], 2335-2368 cm⁻¹ and 1603-1612 cm⁻¹ are associated with N-H vibrations[46], and 1361-1373 cm⁻¹ is due to vibrations of N-O bonds[34]. These initial vibrational bands indicate that after the calcination of the two compounds, the presence of impurities is still found, such as adsorbed water, ammonium ions, and nitro compounds, which are derivatives of the chemical reagents used in the synthesis[34]. The band observed around 2831 cm⁻¹ is mainly present in the FTIR spectra of the sample synthesized by the sol-gel method, suggesting that it may be attributed to traces of by-products from citric acid and ethylene glycol used in the synthesis. The last two absorption bands located around 585-589 cm⁻¹ (υ_1) and 406-408 cm⁻¹ (υ_2), arise from vibrations between the metal cations and oxygen anions of the Ni-Co mixed ferrites. The band υ_1 corresponds to vibrations between the ions situated in the tetrahedral sites of the spinel structure, while υ_2 arises from vibrations of ions with octahedral coordination[47,48]. Therefore, these bands,

attributed to Ni-O, Co-O, and Fe-O vibrations, confirm that the synthesized compounds crystallized in the cubic spinel structure.

Figure 3 shows a TEM image of the $Ni_{0.5}Co_{0.5}Fe_2O_4$ synthesized through the coprecipitation method, while Figure 4 presents an SEM image of the Ni-Co mixed ferrite synthesized via the
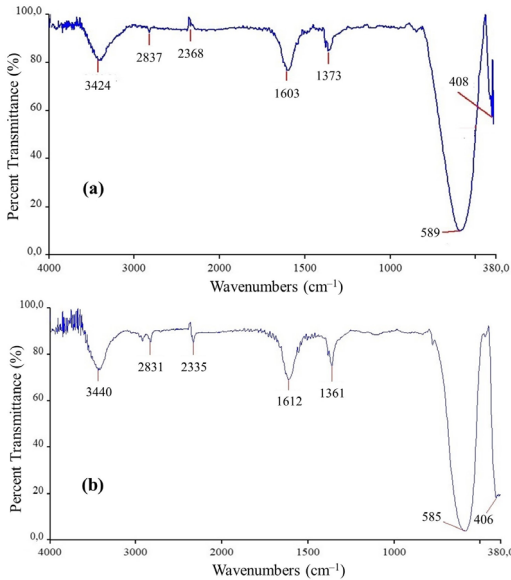
Figure 2. FTIR spectra of $Ni_{0.5}Co_{0.5}Fe_2O_4$ nanopowders synthesized by the (a) coprecipitation and (b) sol-gel methods.
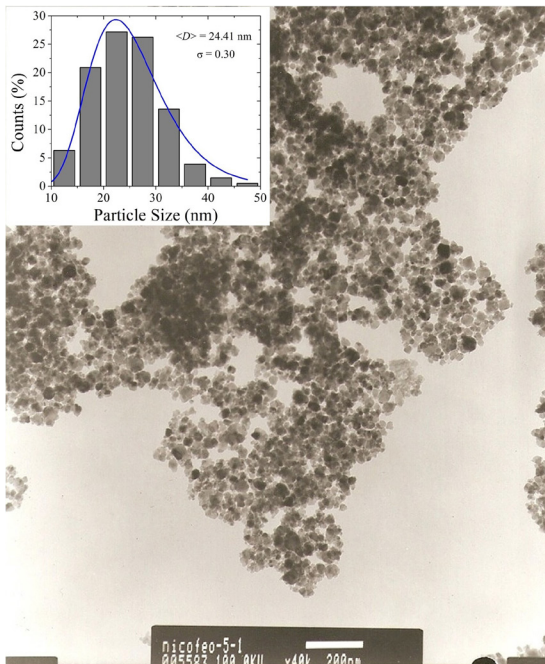
Figure 3. TEM image and size histogram of $Ni_{0.5}Co_{0.5}Fe_2O_4$ nanoparticles synthesized by the coprecipitation method. The scale bar corresponds to 200 nm.

sol-gel method. The micrographs reveal that the synthesized compounds consist of irregularly shaped nanoparticles that are agglomerated. The insets in figures 3 and 4 show the particle size histograms of both compounds, demonstrating that the two ferrites exhibit broad particle size distributions that conform to a Log-normal function. Mean particle sizes of 24 nm and 43 nm were obtained for the compounds synthesized by the coprecipitation and sol-gel methods, respectively. The results indicate that the particles synthesized through the coprecipitation method are smaller than those obtained via the sol-gel method, confirming the findings of the XRD analysis, which were based on the width of the diffraction peaks in both synthesized compounds. When comparing the particle sizes (D) obtained from TEM or SEM with the crystallite sizes (D_{XRD}) calculated using the Scherrer equation, it is observed that the D_{XRD} values are smaller than those of D. This suggests that most of the synthesized nanoparticles consist of a crystalline multidomain structure. These results are consistent with findings in the literature, which generally indicate that particle sizes estimated using the Scherrer equation are smaller than the real sizes observed in TEM or SEM micrographs[49,50]. These discrepancies between D_{XRD} and D values may be attributed to factors such as nanoparticle aggregation, the presence of large particles, and the polydispersity of particle sizes[46,51].

Figure 5 shows the magnetization curves as a function of temperature in the ZFC and FC modes for the nanocompounds synthesized using the coprecipitation and sol-gel methods. The magnetization behavior in both Ni-Co mixed ferrites is similar, with the ZFC and FC curves exhibiting separation throughout the entire temperature range of the measurements, suggesting that the nanoparticles are in the blocked magnetic regime at temperatures below 320 K. The behavior of the FC magnetization indicates the existence of strong magnetic interactions between the nanoparticles in both compounds. This is evident from the decrease in magnetization data as the temperature decreases after cooling the sample under an external magnetic field. This behavior is contrary to what
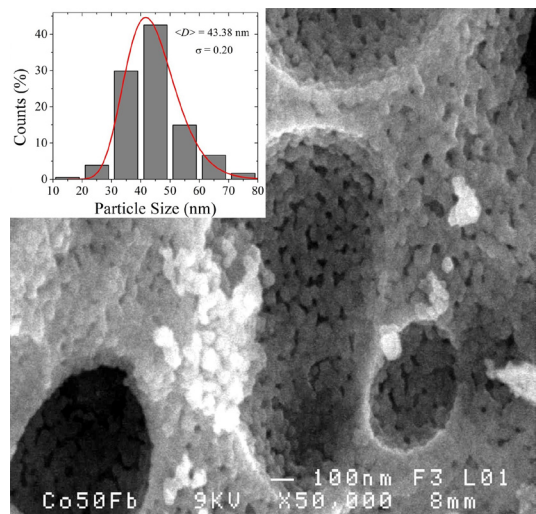
Figure 4. SEM image and size histogram of $Ni_{0.5}Co_{0.5}Fe_2O_4$ nanoparticles synthesized by the sol-gel method.

Structural and Magnetic Characterization of Ni-Co Mixed Ferrite Nanopowders Synthesized via
Coprecipitation and Sol-Gel Methods

5

occurs in a system of non-interacting particles, where the reduction in thermal energy promotes the alignment of magnetic moments in response to a magnetic field, resulting in an increase in FC magnetization as the temperature decreases[52].

Figure 6 shows the magnetization curves as a function of the applied magnetic field, measured at 5 and 320 K, for the $Ni_{0.5}Co_{0.5}Fe_2O_4$ nanoparticles synthesized via the coprecipitation method. In Figure 7, the $M(H)$ curves at 2 and 300 K are presented for the Ni-Co mixed ferrite nanoparticles synthesized using the sol-gel method. In the curves measured at 2 and 5 K, hysteresis cycles with notable coercive fields are clearly observed, indicating that $Ni_{0.5}Co_{0.5}Fe_2O_4$ behaves as a hard magnetic material at low temperatures. The insets in the two figures reveal that even at 300 and 320 K, the Ni-Co mixed ferrite compounds still exhibit magnetic hysteresis, confirming that the nanoparticles maintain their blocked magnetic state up to 320 K and present a magnetic ordering at room temperature. The results suggest that at $T \leq 320$ K, the nanoparticles exhibit magnetic ordering, which is likely to correspond to the ferrimagnetic coupling between the magnetic moments of the metal cations constituting the interior of the particles[53]. In all four hysteresis curves, it is observed that the magnetic saturation state was not reached even with the application of magnetic fields of up to 55 kOe. Therefore, the M_S values were estimated by extrapolating the magnetization data to an infinite field. This was achieved by plotting the magnetization as a function of $1/H$ and performing a linear fit of the magnetization data as $1/H$ tends to zero. The M_S values were determined from the equation:

$$M = M_S(1 - \beta / H) \tag{4}$$

Where β is a magnetic field-independent parameter[34].

Table 1 presents the values for coercive field, remanent magnetization, and saturation magnetization of the $Ni_{0.5}Co_{0.5}Fe_2O_4$ nanoparticulate powders synthesized using the coprecipitation and sol-gel methods. The errors of the calculated M_S values are also presented in the last column of Table 1. It can be observed that both samples exhibit similar magnetic properties, as the values of M_S, M_R, and H_C obtained at low temperatures are comparable to each other, as are the values of these parameters determined at high temperatures. The M_S and H_C values are close to those reported in other investigations of the magnetic properties of $Ni_{0.5}Co_{0.5}Fe_2O_4$ nanoparticles[54,55]. The saturation magnetization values obtained are higher than those known for bulk Ni ferrite, which are 56 emu/g (at 0 K) and 50 emu/g (at 293 K)[56], but lower than those of cobalt ferrite. This is consistent with the fact that the synthesized material is a mixed Ni-Co ferrite.

The inversion parameter (δ) of the spinel structure, in which the two Ni-Co mixed ferrite nanocompounds have crystallized, was calculated based on the saturation magnetization values determined at low temperatures. The distribution of divalent cations A (Ni^{2+} and Co^{2+}) and
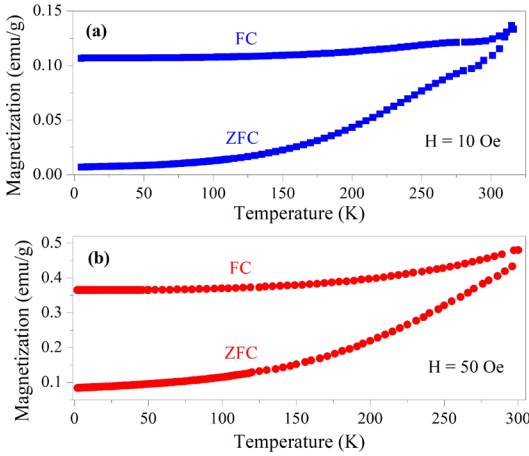
Figure 5. Temperature dependence of the ZFC and FC magnetizations of the $Ni_{0.5}Co_{0.5}Fe_2O_4$ nanoparticles synthesized by the (a) coprecipitation and (b) sol-gel methods.
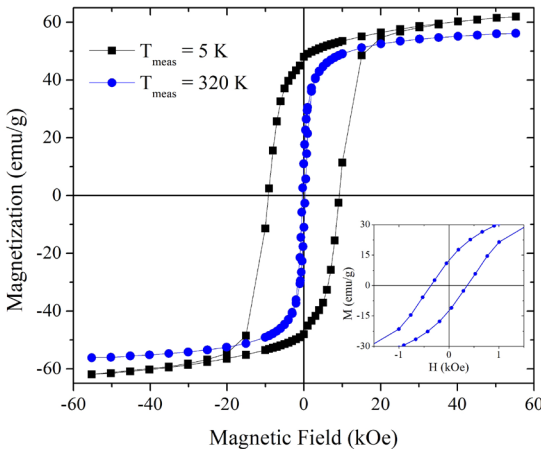
Figure 6. Magnetic field dependence of magnetization, measured at 5 and 320 K, of $Ni_{0.5}Co_{0.5}Fe_2O_4$ nanoparticles synthesized by the coprecipitation method. The inset shows the $M(H)$ curve at 320 K in the region of a small applied field.
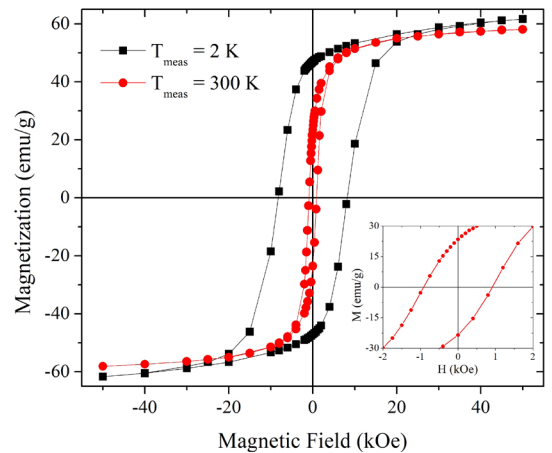
Figure 7. Magnetic field dependence of magnetization, measured at 2 and 300 K, of $Ni_{0.5}Co_{0.5}Fe_2O_4$ nanoparticles synthesized by the sol-gel method. The inset shows the $M(H)$ curve at 300 K in the region of a small applied field.

Table 1. Coercive Field (H_C), Remanent Magnetization (M_R), and Saturation Magnetization (M_S), Measured at Different Temperatures (T_{meas}), of the Ni-Co Mixed Ferrite Nanopowders Synthesized by Coprecipitation and Sol-Gel Methods.

Synthesis method	T_{meas} (K)	H_C (Oe)	M_R (emu/g)	M_S (emu/g)
Coprecipitation	5	9224	48.01	63.94 ± 0.43
	320	365	10.98	57.81 ± 0.18
Sol-gel	2	8202	46.93	64.88 ± 0.47
	300	917	23.46	60.57 ± 0.22

Table 2. Comparison of Cationic Distribution of $Ni_{0.5}Co_{0.5}Fe_2O_4$ Nanoparticles Synthesized by Different Methods.

Synthesis method	Cation distribution		Reference
	t-site	*o*-site	
Coprecipitation	$Co_{0.05}Fe_{0.95}$	$Ni_{0.5}Co_{0.45}Fe_{1.05}$	This work
Sol-gel	$Co_{0.06}Fe_{0.94}$	$Ni_{0.5}Co_{0.44}Fe_{1.06}$	This work
Ultrasonic technique	$Ni_{0.1}Co_{0.1}Fe_{0.8}$	$Ni_{0.4}Co_{0.4}Fe_{1.2}$	Almessiere et al.[26]
Sol-gel auto-combustion	$Ni_{0.1}Co_{0.1}Fe_{0.8}$	$Ni_{0.4}Co_{0.4}Fe_{1.2}$	Kadam et al.[27]
Grinding	Fe	$Ni_{0.5}Co_{0.5}Fe$	Lee and Lee[61]

trivalent cations Fe^{3+} between the tetrahedral and octahedral sites of the spinel structure, which is determined by δ, can be represented by the formula $[A_{1-\delta}Fe_\delta]^T [A_\delta Fe_{2-\delta}]^O O_4$, where the superscripts *t* and *o* indicate the tetrahedral and octahedral positions, respectively. At temperatures close to 0 K, it can be assumed that inside the nanoparticles, the magnetic moments are ordered, presenting a collinear ferrimagnetic arrangement composed of two magnetic sublattices formed by the cations located in the tetrahedral and octahedral sites of the spinel structure[57]. Considering the preference of Ni^{2+} cations to locate in the octahedral coordination sites of the spinel structure[58], the magnetic moment per formula unit (μ_{fu}) of $Ni_{0.5}Co_{0.5}Fe_2O_4$ ferrite can be represented by the equation:

$$\mu_{fu} = \left[0.5 \cdot \mu_{Ni} + (\delta - 0.5) \cdot \mu_{Co} + (2 - \delta) \cdot \mu_{Fe} \right]^o - \left[(1 - \delta) \cdot \mu_{Co} + \delta \cdot \mu_{Fe} \right]^t \quad (5)$$

Where μ_{Ni}, μ_{Co}, and μ_{Fe} correspond to the spin-only magnetic moments of Ni^{2+}, Co^{2+}, and Fe^{3+} ions, which are 2 μ_B, 3 μ_B, and 5 μ_B, respectively[56]. The values of μ_{fu} corresponding to M_S (at 2 and 5 K) are 2.69 μ_B and 2.72 μ_B for the Ni-Co mixed ferrite synthesized by the coprecipitation and sol-gel methods, respectively. The inversion parameter obtained is δ = 0.95 for the $Ni_{0.5}Co_{0.5}Fe_2O_4$ synthesized by the coprecipitation method, and δ = 0.94 for the mixed ferrite produced by the sol-gel method. Therefore, the synthesized nanocompounds present a spinel structure with a high degree of inversion, which falls intermediate to the known δ values for $NiFe_2O_4$ and $CoFe_2O_4$[59,60].

Table 2 compares the cationic distributions obtained in this work with those reported in previous investigations, which were determined through structural refinements from XRD data or Mössbauer spectra analysis. Almessiere et al.[26] and Kadam et al.[27] reported similar cationic distributions corresponding to a partially inverse spinel structure, with 80% of the Ni^{2+}

and Co^{2+} cations located in the octahedral sites. Lee and Lee[61], on the other hand, reported that 100% of the divalent cations are located in the octahedral sites, forming an inverse spinel structure identical to that of Ni ferrite. In this research, an intermediate result between those reported in the literature was obtained: 100% of the Ni^{2+} cations are located in the octahedral sites, while the proportion of Co^{2+} cations located in the octahedral positions corresponds to 90% and 88% for mixed Ni-Co ferrite synthesized by coprecipitation and sol-gel methods, respectively.

4. Conclusions

$Ni_{0.5}Co_{0.5}Fe_2O_4$ nanoparticulate powders were synthesized using the coprecipitation and sol-gel methods, and they exhibited similar structural and magnetic characteristics. The synthesized compounds presented a single crystalline phase corresponding to the cubic spinel structure, with a lattice parameter of approximately 8.35 Å, and a high degree of inversion (with δ ranging between 0.94 and 0.95). In both compounds, the particles agglomerated to form nanoaggregates. However, the mean size of the particles synthesized by the coprecipitation method was smaller (24 nm) compared to those produced by the sol-gel method (43 nm). Both nanocompounds exhibited ordered magnetic behavior at temperatures below 320 K, indicating that the nanoparticles were in the blocked magnetic regime. Furthermore, the presence of strong magnetic interactions between the particles was evident, as they agglomerated to form nanoparticle aggregates.

5. Acknowledgments

6. References

1. Keshri S, Biswas S. Synthesis, physical properties, and biomedical applications of magnetic nanoparticles: a review. Prog Biomater. 2022;11(4):347-72. http://dx.doi.org/10.1007/s40204-022-00204-8.

2. Mahmood A, Maqsood A. High-frequency dielectric response of 3d metal (Mn and Cu) doped zinc ferrite nanoparticles for microwave applications. Mater Today Commun. 2023;34:105042. http://dx.doi.org/10.1016/j.mtcomm.2022.105042.

3. Cardoso VF, Francesko A, Ribeiro C, Bañobre-López M, Martins P, Lanceros-Mendez S. Advances in magnetic nanoparticles for biomedical applications. Adv Healthc Mater. 2018;7(5):1700845. http://dx.doi.org/10.1002/adhm.201700845.

4. Wu W, Wu Z, Yu T, Jiang C, Kim WS. Recent progress on magnetic iron oxide nanoparticles: synthesis, surface functional strategies and biomedical applications. Sci Technol Adv Mater. 2015;16(2):023501. http://dx.doi.org/10.1088/1468-6996/16/2/023501.

5. Sheikh FA, Khan Asghar HMN ul H, Khalid M, Gilani ZA, Ali SM, Khan N ul H, et al. Dielectrically modified Dy3+ substituted nickel-cobalt ferrites for high frequency devices. Physica B. 2023;652:414656. http://dx.doi.org/10.1016/j.physb.2023.414656.

6. Elsi S, Mohanapriya S, Pushpanathan K. Observation of novel superparamagnetism in ZnS:Co quantum dots. J Supercond Nov Magn. 2020;33(10):3223-40. http://dx.doi.org/10.1007/s10948-020-05573-4.

7. Abdel Maksoud MIA, Fahim RA, Bedir AG, Osman AI, Abouelela MM, El-Sayyad GS, et al. Engineered magnetic oxides nanoparticles as efficient sorbents for wastewater remediation: a review. Environ Chem Lett. 2022;20(1):519-62. http://dx.doi.org/10.1007/s10311-021-01351-3.

8. Fino D, Russo N, Saracco G, Specchia V. Removal of NOx and diesel soot over catalytic traps based on spinel-type oxides. Powder Technol. 2008;180(1-2):74-8. http://dx.doi.org/10.1016/j.powtec.2007.03.003.

9. Fino D, Russo N, Saracco G, Specchia V. Catalytic removal of NOx and diesel soot over nanostructured spinel-type oxides. J Catal. 2006;242(1):38-47. http://dx.doi.org/10.1016/j.jcat.2006.05.023.

10. Singh D, Gurjar BR. Recent innovation and impacts of nano-based technologies for wastewater treatment on humans: a review. Environ Monit Assess. 2023;195(3):357. http://dx.doi.org/10.1007/s10661-022-10790-6.

11. Márquez G, Sagredo V, Guillen-Guillen R. Structural characterization, magnetic properties, and heating power of nickel ferrite nanoparticles. IEEE Trans Magn. 2019;55(12):1-7. http://dx.doi.org/10.1109/TMAG.2019.2939118.

12. Ferreira TAS, Waerenborgh JC, Mendonça MHRM, Nunes MR, Costa FM. Structural and morphological characterization of FeCo2O4 and CoFe2O4 spinels prepared by a coprecipitation method. Solid State Sci. 2003;5(2):383-92. http://dx.doi.org/10.1016/S1293-2558(03)00011-6.

13. Mozaffari M, Amighian J, Darsheshdar E. Magnetic and structural studies of nickel-substituted cobalt ferrite nanoparticles, synthesized by the sol–gel method. J Magn Magn Mater. 2014;350:19-22. http://dx.doi.org/10.1016/j.jmmm.2013.08.008.

14. Márquez G, Sagredo V. Effect of the substitution of co by ni on the crystal structure and magnetic properties of cobalt ferrite nanoparticles. In: Proceedings of the 21th LACCEI International Multi-Conference for Engineering, Education and Technology (LACCEI 2023). Latin American and Caribbean Consortium of Engineering Institutions; 2023; Buenos Aires. Buenos Aires: CONFEDI. p. 1-6. https://doi.org/10.18687/LACCEI2023.1.1.1438.

15. Mathew DS, Juang RS. An overview of the structure and magnetism of spinel ferrite nanoparticles and their synthesis in microemulsions. Chem Eng J. 2007;129(1-3):51-65. http://dx.doi.org/10.1016/j.cej.2006.11.001.

16. Sharifi I, Shokrollahi H, Amiri S. Ferrite-based magnetic nanofluids used in hyperthermia applications. J Magn Magn Mater. 2012;324(6):903-15. http://dx.doi.org/10.1016/j.jmmm.2011.10.017.

17. Majetich SA, Wen T, Mefford OT. Magnetic nanoparticles. MRS Bull. 2013;38(11):899-903. http://dx.doi.org/10.1557/mrs.2013.230.

18. Bedanta S, Kleemann W. Supermagnetism. J Phys D Appl Phys. 2009;42(1):1-28. http://dx.doi.org/10.1088/0022-3727/42/1/013001.

19. Santiago E, Marquez G, Guillen-Guillen R, Jaimes C, Sagredo V, Delgado GE. Characterization of hematite and Ni-Zn mixed ferrites nanocomposites synthesized by the coprecipitation method. Rev Latinoam Metal Mater. 2020;40(1):49-58.

20. Zhao Y. Co-precipitated Ni/Mn shell coated nano Cu-rich core structure: a phase-field study. J Mater Res Technol. 2022;21:546-60. http://dx.doi.org/10.1016/j.jmrt.2022.09.032.

21. Srivastava M, Chaubey S, Ojha AK. Investigation on size dependent structural and magnetic behavior of nickel ferrite nanoparticles prepared by sol–gel and hydrothermal methods. Mater Chem Phys. 2009;118(1):174-80. http://dx.doi.org/10.1016/j.matchemphys.2009.07.023.

22. Shirsath SE, Wang D, Jadhav SS, Mane ML, Li S. Ferrites obtained by sol-gel method. In: Klein L, Aparicio M, Jitianu A, editors. Handbook of sol-gel science and technology: processing, characterization and applications. Cham: Springer International Publishing; 2018. p. 695–735.

23. Samoila P, Cojocaru C, Simionescu M, Sacarescu G, Roman G, Enache AC, et al. Cobalt ferrite particles produced by sol-gel autocombustion and embedded in polysilane: an innovative route to magnetically-induced fluorescence composites. Molecules. 2022;27(19):6393. http://dx.doi.org/10.3390/molecules27196393.

24. Nguyen AT, Nguyen TD, Mittova VO, Berezhnaya MV, Mittova IY. Phase composition and magnetic properties of Ni1-xCoxFe2O4 nanocrystals with spinel structure, synthesized by Co-precipiation. Nanosyst Physics, Chem Math. 2017;371-7. https://doi.org/10.17586/2220-8054-2017-8-3-371-377.

25. Torkian S, Ghasemi A, Shoja Razavi R. Cation distribution and magnetic analysis of wideband microwave absorptive CoxNi1−xFe2O4 ferrites. Ceram Int. 2017;43(9):6987-95. http://dx.doi.org/10.1016/j.ceramint.2017.02.124.

26. Almessiere MA, Slimani Y, Auwal İA, Shirsath SE, Manikandan A, Baykal A, et al. Impact of Tm3+ and Tb3+ rare earth cations substitution on the structure and magnetic parameters of Co-Ni nanospinel ferrite. Nanomaterials (Basel). 2020;10(12):2384. http://dx.doi.org/10.3390/nano10122384.

27. Kadam RH, Birajdar AP, Alone ST, Shirsath SE. Fabrication of Co0.5Ni0.5CrxFe2−xO4 materials via sol–gel method and their characterizations. J Magn Magn Mater. 2013;327:167-71. http://dx.doi.org/10.1016/j.jmmm.2012.09.059.

28. Phugate DV, Borade RB, Kadam SB, Dhale LA, Kadam RH, Shirsath SE, et al. Effect of Ho3+ Ion doping on thermal, structural, and morphological properties of Co–Ni ferrite synthesized by sol-gel method. J Supercond Nov Magn. 2020;33(11):3545-54. http://dx.doi.org/10.1007/s10948-020-05616-w.

29. Babu KV, Sailaja B, Jalaiah K, Shibeshi PT, Ravi M. Effect of zinc substitution on the structural, electrical and magnetic properties of nano-structured Ni0.5Co0.5Fe2O4 ferrites. Physica B. 2018;534:83-9. http://dx.doi.org/10.1016/j.physb.2018.01.022.

30. Kokare MK, Jadhav NA, Kumar Y, Jadhav KM, Rathod SM. Effect of Nd3+ doping on structural and magnetic properties of Ni0.5Co0.5Fe2O4 nanocrystalline ferrites synthesized by sol-gel auto combustion method. J Alloys Compd. 2018;748:1053-61. http://dx.doi.org/10.1016/j.jallcom.2018.03.168.

31. Maaz K, Karim S, Lee KJ, Jung MH, Kim GH. Effect of temperature on the magnetic characteristics of Ni0.5Co0.5Fe2O4

nanoparticles. Mater Chem Phys. 2012;133(2-3):1006-10. http://dx.doi.org/10.1016/j.matchemphys.2012.02.007.

32. Kour S, Mukherjee R, Kumar N. Synthesis of Ni0.5Co0.5Fe2O4 ferrite and effect of annealing temperature on the structural, morphological and dielectric analysis. ECS Trans. 2022;107(1):19791-801. http://dx.doi.org/10.1149/10701.19791ecst.

33. Choudhary BL, Kumar U, Kumar S, Chander S, Kumar S, Dalela S, et al. Irreversible magnetic behavior with temperature variation of Ni0.5Co0.5Fe2O4 nanoparticles. J Magn Magn Mater. 2020;507:166861. http://dx.doi.org/10.1016/j.jmmm.2020.166861.

34. Márquez G, Sagredo V, Guillén-Guillén R, Attolini G, Bolzoni F. Calcination effects on the crystal structure and magnetic properties of CoFe2O4 nanopowders synthesized by the coprecipitation method. Rev Mex Física. 2020;66:251-7. https://doi.org/10.31349/RevMexFis.66.251.

35. Pérez E, Márquez G, Sagredo V. Effect of calcination on characteristics of nickel ferrite nanoparticles synthesized by sol- gel method. Iraqi J Appl Phys. 2019;15(1):13-7.

36. Khan A, Valicsek Z, Horváth O. Effect of calcination temperature on the structural and photocatalytic properties of iron(II)-doped copper ferrite $Cu^{II}_{0.4}Fe^{II}_{0.6}FeI^{II}_{2}O_{4}$. Mater Lett. 2023;341:134212. http://dx.doi.org/10.1016/j.matlet.2023.134212.

37. Kuekha R, Mubarak TH, Azhdar B. Synthesis, structural, magnetic, and dielectric properties of Ni2+, Mn2+ Co-substituted CoFe2O4 nanoferrites using sol–gel auto combustion method. Mater Sci Eng B. 2023;292:116411. http://dx.doi.org/10.1016/j.mseb.2023.116411.

38. El Moussaoui H, Mahfoud T, Habouti S, El Maalam K, Ben Ali M, Hamedoun M, et al. Synthesis and magnetic properties of tin spinel ferrites doped manganese. J Magn Magn Mater. 2016;405:181-6. http://dx.doi.org/10.1016/j.jmmm.2015.12.059.

39. Godara SK, Kaur V, Narang SB, Singh G, Singh M, Bhadu GR, et al. Tailoring the magnetic properties of M-type strontium ferrite with synergistic effect of co-substitution and calcinations temperature. J Asian Ceram Soc. 2021;9(2):686-98. http://dx.doi.org/10.1080/21870764.2021.1911059.

40. Scherrer P. Bestimmung der Größe und der inneren Struktur von Kolloidteilchen mittels Röntgenstrahlen. Nachrichten von der Gesellschaft der Wissenschaften zu Göttingen, Math Klasse. 1918;1918:98-100.

41. Klug HP, Alexander LE. X-Ray diffraction procedures: for polycrystalline and amorphous materials. 2nd ed. New York: Wiley-VCH; 1974. 992 p.

42. Praphawatvet T, Williams RO. Precipitation technologies for nanoparticle production. In: Williams RO III, Davis DA Jr, Miller DA, editors. Formulating poorly water soluble drugs AAPS advances in the pharmaceutical sciences series. Cham: Springer; 2022. p. 529-98. https://doi.org/10.1007/978-3-030-88719-3_12.

43. Smolkova IS, Kazantseva NE, Parmar H, Babayan V, Smolka P, Saha P. Correlation between coprecipitation reaction course and magneto-structural properties of iron oxide nanoparticles. Mater Chem Phys. 2015;155:178-90. http://dx.doi.org/10.1016/j.matchemphys.2015.02.022.

44. Sanchez Mendez M, Jia Z, Traore M, Ben Amar M, Nikravech M, Kanaev A. Nucleation and growth of mixed vanadium-titanium oxo-alkoxy nanoparticles in sol-gel synthesis. Colloids Surf A Physicochem Eng Asp. 2021;610:125636. http://dx.doi.org/10.1016/j.colsurfa.2020.125636.

45. Pitsevich GA, Doroshenko IY, Pogorelov VE, Shablinskas V, Balevichus V, Kozlovskaya EN. Nonempiric Anharmonic Computations of IR Spectra of Ethanol Conformers in B3LYP/cc-pVQZ Approximation (Stretch C-H Vibrations). Am J Chem. 2012;2(4):218-27. http://dx.doi.org/10.5923/j.chemistry.20120204.06.

46. Morales F, Márquez G, Sagredo V, Torres TE, Denardin JC. Structural and magnetic properties of silica-coated magnetite

nanoaggregates. Physica B. 2019;572:214-9. http://dx.doi.org/10.1016/j.physb.2019.08.007.

47. Waldron RD. Infrared spectra of ferrites. Phys Rev. 1955;99(6):1727-35. http://dx.doi.org/10.1103/PhysRev.99.1727.

48. Ati AA, Othaman Z, Samavati A. Influence of cobalt on structural and magnetic properties of nickel ferrite nanoparticles. J Mol Struct. 2013;1052:177-82. http://dx.doi.org/10.1016/j.molstruc.2013.08.040.

49. Mbarek F, Chérif I, Chérif A, Alonso JM, Morales I, de la Presa P, et al. Insights into the synthesis parameters effects on the structural, morphological, and magnetic properties of copper oxide nanoparticles. Materials (Basel). 2023;16(9):3426. http://dx.doi.org/10.3390/ma16093426.

50. Patsula V, Moskvin M, Dutz S, Horák D. Size-dependent magnetic properties of iron oxide nanoparticles. J Phys Chem Solids. 2016;88:24-30. http://dx.doi.org/10.1016/j.jpcs.2015.09.008.

51. Canchanya-Huaman Y, Mayta-Armas AF, Pomalaya-Velasco J, Bendezú-Roca Y, Guerra JA, Ramos-Guivar JA. Strain and grain size determination of CeO2 and TiO2 nanoparticles: comparing integral breadth methods versus rietveld, μ-Raman, and TEM. Nanomaterials (Basel). 2021;11(9):2311. http://dx.doi.org/10.3390/nano11092311.

52. Knobel M, Nunes WC, Socolovsky LM, De Biasi E, Vargas JM, Denardin JC. Superparamagnetism and other magnetic features in granular materials: a review on ideal and real systems. J Nanosci Nanotechnol. 2008;8(6):2836-57. http://dx.doi.org/10.1166/jnn.2008.15348.

53. Hedayatnasab Z, Abnisa F, Daud WMAW. Review on magnetic nanoparticles for magnetic nanofluid hyperthermia application. Mater Des. 2017;123:174-96. http://dx.doi.org/10.1016/j.matdes.2017.03.036.

54. Mohammed OH, Jassim AS, Fathi SJ. Effect of laser on magnetic properties of nano composite material ($Ni_{0.5}Co_{0.5}Fe_2O_4$) prepared by sol–gel. Mater Today Proc. 2022;61:921-4. http://dx.doi.org/10.1016/j.matpr.2021.10.099.

55. Sun J, Chen J, Ge H, Sun H, Yang Y, Zhang Y. Biomass-derived carbon decorated with $Ni_{0.5}Co_{0.5}Fe_2O_4$ particles towards excellent microwave absorption performance. Compos Part A Appl Sci Manuf. 2022;156:106850. https://doi.org/10.1016/j.compositesa.2022.106850.

56. Cullity BD, Graham CD. Introduction to magnetic materials. 2nd ed. New York: IEEE Press; 2009. 568 p.

57. Muscas G, Yaacoub N, Concas G, Sayed F, Sayed Hassan R, Greneche JM, et al. Evolution of the magnetic structure with chemical composition in spinel iron oxide nanoparticles. Nanoscale. 2015;7(32):13576-85. http://dx.doi.org/10.1039/C5NR02723C.

58. Hölscher J, Andersen HL, Saura-Múzquiz M, Garbus PG, Christensen M. Correlation between microstructure, cation distribution and magnetism in Ni1−xZnxFe2O4 nanocrystallites. CrystEngComm. 2020;22(3):515-24. http://dx.doi.org/10.1039/C9CE01324E.

59. Andersen HL, Saura-Múzquiz M, Granados-Miralles C, Canévet E, Lock N, Christensen M. Crystalline and magnetic structure–property relationship in spinel ferrite nanoparticles. Nanoscale. 2018;10(31):14902-14. http://dx.doi.org/10.1039/C8NR01534A.

60. Harada M, Kuwa M, Sato R, Teranishi T, Takahashi M, Maenosono S. Cation distribution in monodispersed MFe2O4 (M = Mn, Fe, Co, Ni, and Zn) nanoparticles investigated by X-ray absorption fine structure spectroscopy: implications for magnetic data storage, catalysts, sensors, and ferrofluids. ACS Appl Nano Mater. 2020;3(8):8389-402. http://dx.doi.org/10.1021/acsanm.0c01810.

61. Lee CS, Lee CY. Superexchange interactions in $Ni_{0.5}Co_{0.5}Fe_2O_4$. J Appl Phys. 1996;79(8):5710-2. http://dx.doi.org/10.1063/1.361840.